Oceanic Influence on Seasonal Malaria Incidence in West Africa

IBRAHIMA DIOUF,[a,i] ROBERTO SUÁREZ-MORENO,[b] BELEN RODRÍGUEZ-FONSECA,[c,d] CYRIL CAMINADE,[e] MALICK WADE,[f] WASSILA M. THIAW,[a] ABDOULAYE DEME,[f] ANDREW P. MORSE,[g] JAQUES-ANDRÉ NDIONE,[h] AMADOU T. GAYE,[i] ANTA DIAW,[j] AND MARIE KHEMESSE NGOM NDIAYE[j]

[a] *NOAA/Center for Weather and Climate Prediction, College Park, Maryland*
[b] *Lamont-Doherty Earth Observatory, Columbia University, Palisades, New York*
[c] *Facultad de Físicas Departamento de Meteorología, Universidad Complutense de Madrid, Madrid, Spain*
[d] *Instituto de Geociencias, Agencia Estatal del Consejo Superior de Investigaciones Cientficas, Universidad Complutense de Madrid, Madrid, Spain*
[e] *Department of Livestock and One Health, Institute of Infection, Veterinary and Ecological Sciences, University of Liverpool, Liverpool, United Kingdom*
[f] *Unité de Formation et de Recherche de Sciences Appliquées et de Technologie, Université Gaston Berger, Saint-Louis, Senegal*
[g] *Department of Geography and Planning, School of Environmental Sciences, University of Liverpool, Liverpool, United Kingdom*
[h] *Centre de Suivi Ecologique, Dakar, Senegal*
[i] *Laboratoire de Physique de l'Atmosphère et de l'Océan–Siméon Fongang, Ecole Supérieure Polytechnique de l'Université Cheikh Anta Diop, Dakar-Fann, Dakar, Senegal*
[j] *General Direction of Public Health, Ministry of Health and Social Action, Dakar, Senegal*

(Manuscript received 10 October 2020, in final form 4 November 2021)

ABSTRACT: Climate variability is a key factor in driving malaria outbreaks. As shown in previous studies, climate-driven malaria modeling provides a better understanding of malaria transmission dynamics, generating malaria-related parameters validated as a reliable benchmark to assess the impact of climate on malaria. In this framework, the present study uses climate observations and reanalysis products to evaluate the predictability of malaria incidence in West Africa. Sea surface temperatures (SSTs) are shown as a skillful predictor of malaria incidence, which is derived from climate-driven simulations with the Liverpool Malaria Model (LMM). Using the SST-based Statistical Seasonal Forecast model (S4CAST) tool, we find robust modes of anomalous SST variability associated with skillful predictability of malaria incidence Accordingly, significant SST anomalies in the tropical Pacific and Atlantic Ocean basins are related to a significant response of malaria incidence over West Africa. For the Mediterranean Sea, warm SST anomalies are responsible for increased surface air temperatures and precipitation over West Africa, resulting in higher malaria incidence; conversely, cold SST anomalies are responsible for decreased surface air temperatures and precipitation over West Africa, resulting in lower malaria incidence.. Our results put forward the key role of SST variability as a source of predictability of malaria incidence, being of paramount interest to decision-makers who plan public health measures against malaria in West Africa. Accordingly, SST anomalies could be used operationally to forecast malaria risk over West Africa for early warning systems.

KEYWORDS: Atmosphere; Ocean; Africa; Climate prediction; Climate variability; Oceanic variability

1. Introduction

Malaria is spread by the bite of a female *Anopheles* mosquito mainly in tropical and subtropical regions (Pene et al. 1967; Carnevale et al. 1984). The disease can cause fever, chills, and flu-like illnesses, and if not treated in time, it may cause severe complications and even death. Indeed, about 409 000 people die of malaria each year, with 90% of cases occurring in sub-Saharan Africa (Kiszewski and Teklehaimanot 2004; Walker et al. 2007; World Health Organization 2019, 2020). The most vulnerable people are children under 5 years of age and pregnant women (Korenromp et al. 2003; Breman et al. 2004; World Health Organization 2008; Ouédraogo et al. 2011). Many external factors interact to determine malaria transmission, including socioeconomic parameters (Cleaver 1977; Sachs and Malaney 2002) and climate variability (Lindsay and Birley 1996; Ndiaye et al. 2001) at both local and regional scales.

In Africa, malaria outbreaks are conditioned by surface air temperature, humidity, and rainfall (e.g., Gage et al. 2008; Arab et al. 2014). Relative humidity above 60% due to rainfall, combined with a range of medium-to-high temperatures (18°–32°C), and conducive vegetation foment the proliferation of malaria-transmitting mosquitoes, leading to an increase in malaria incidence in several African regions (Craig et al. 1999; Liu et al. 2011). In particular, temperatures are a critical factor for the transmission of vector-borne diseases (Luterbacher et al. 2004; Rogers and Randolph 2000; Wilson et al. 1998; Freeman and Bradley 1996; Bayoh 2001). At temperatures below 18°C, *Plasmodium falciparum*, which causes the most prevalent and lethal form of malaria in Africa, cannot complete its sporogonic cycle in the *Anopheles* mosquito and thus cannot be transmitted (Patz and Olson 2006).

Supplemental information related to this paper is available at the Journals Online website: https://doi.org/10.1175/WCAS-D-20-0160.s1.

Corresponding author: Ibrahima Diouf, ibrahima.diouf@noaa.gov

DOI: 10.1175/WCAS-D-20-0160.1

Accordingly, moderate malaria transmission occurs over Africa's northern and southern fringes (Hay et al. 2005). In contrast, the Sahara Desert is usually malaria free because it is too hot and dry, with very low humidity. These conditions are consistent with the optimum temperature for malaria transmission of approximately 27°C (Mordecai et al. 2013) and the upper temperature threshold for malaria vector survival of approximately 35°C (Mordecai et al. 2019).

Climate variability in the West African Sahel is strongly influenced by anomalous sea surface temperatures (SST) in terms of the so-called SST-forced atmospheric teleconnections. In particular, the variability of rainfall and surface air temperatures is driven by remote and nearby SST anomalies (Losada et al. 2010ab; Rodríguez-Fonseca et al. 2011, 2015; Suárez-Moreno et al. 2018; among others). The leading SST modes of variability known to impact monsoon rainfall in the Sahel are El Niño–Southern Oscillation (ENSO) in the tropical Pacific Ocean, the Atlantic equatorial mode (AEM; also known as the Atlantic Niño), and Mediterranean SST variability (e.g., Polo et al. 2008; Mohino et al. 2011; Losada et al. 2012). SST anomalies therefore emerge as a potential source of predictability for malaria outbreaks. In this context, previous studies investigated the links between large-scale modes of SST variability and malaria-related parameters, particularly those related to the ENSO. The ENSO develops over the tropical Pacific and influences global climate variability (e.g., Philander 1983). Former studies demonstrated that malaria mortality and morbidity increase by an average of about one-third in the year following an El Niño event (warm phase of ENSO) over Venezuela and Colombia (Bouma and Dye 1997; Bouma et al. 1997; Gagnon et al. 2002). Similarly, Githeko and Ndegwa (2001) showed that El Niño led to floods and malaria outbreaks in Kenya. While associated with floods in East Africa, El Niño is generally linked to drier conditions in West Africa. Prost (1991) found a relationship between ENSO and specific diseases like malaria outbreaks during the 1970s, corresponding to persistent drought in the Sahel. Nevertheless, other local factors (socioeconomic conditions, resistance to insecticide or drugs, etc.) were likely to be preexisting because malaria prevalence remained high, despite the observed reduction in rainfall.

Motivated by the factors raised above, this study is conceived as a continuation of the preliminary work carried out within the Quantifying Weather and Climate Impacts on Health in Developing Countries (QWeCI) project in the context of the European Union's funded research (EU FP7 project). The QWeCI project aimed to understand the climate drivers of vector-borne diseases to generate an integrated decision support framework for climate and weather impacts on health (Morse et al. 2012). Earlier work on forecasting malaria epidemics based on seasonal forecasts of climate variability was carried out by Tompkins and Di Giuseppe (2015) and Tompkins et al. (2019). In West Africa, the risk of malaria transmission is primarily associated with rainfall and temperature, with a 2-month lag observed between the maximum rainfall in August and the peak in malaria cases in October (Diouf et al. 2013, 2017, 2020). The reliability of the simulated malaria incidence time series was validated using observed malaria data (Diouf et al. 2020) from the surveillance system run by the National Malaria Control Programme [in French: Programme National de Lutte Contre le Paludisme (PNLP)] for Senegal.

In this study, we analyze the potential seasonal predictability of malaria incidence associated with the leading modes of interannual SST variability known to impact climate variability in West Africa. Malaria incidence is simulated with the Liverpool Malaria Model (LMM), a dynamic malaria model driven by a daily time series of rainfall and 2-m surface temperatures (Hoshen and Morse 2004). Specifically, three climate reanalyses are used to run the LMM that provide different malaria incidence outputs. The SST-based Statistical Seasonal Forecast model (S4CAST; Suárez-Moreno and Rodríguez-Fonseca 2015) is then used to analyze the leading covariability patterns between SST anomalies and anomalous malaria incidence to determine skillful ocean predictors. Relative to previous works, we go one step farther by estimating the impact of SSTs on simulated malaria incidence, exploring the role of the ocean–atmosphere interactions in driving the effects of climate variability on malaria. Our work is structured as follows: section 2 is dedicated to the data and method, and sections 3 and 4 are devoted to results and validation, respectively. Section 5 focuses on the discussion and conclusions.

2. Data and method

a. Data

This study focuses on the West African region (4°–18°N, 20°W–15°E; see Fig. 1a). Specifically, we look at malaria incidence (%; i.e., cases per 100 people) as simulated by the LMM (Hoshen et al. 2004), which is driven by daily rainfall and temperature data from different reanalysis datasets. The full periods, spatial resolutions, and references of these reanalyses are shown in Fig. 1b. We note that, the time series of simulated malaria incidence derived from the climate reanalysis datasets were previously validated using surveillance malaria data for Senegal (Diouf et al. 2020). These data were recorded by the PNLP, and all age groups were screened. The number of observed malaria cases was available for various health districts in Senegal for the period 2001–10. These malaria data were recorded and averaged from 11 main sites (Dakar, Diourbel, Fatick, Kaolack, Kolda, Louga, Matam, Saint-Louis, Tambacounda, Thies, and Ziguinchor) for all health districts and hospitals to derive monthly time series. Validation of seasonal and interannual cycles of simulated malaria incidence was performed.

In our study, we expressly use the following reanalysis datasets: the Twentieth Century Reanalysis (20CR) spanning the period 1910–2009 at 2.5° × 2.5° spatial resolution (Compo et al. 2011) and the National Centers for Environmental Prediction (NCEP) Reanalysis (Kalnay et al. 1996) for the period 1948–2017 at 2.5° × 2.5° spatial resolution. These two reanalysis datasets are provided by the National Oceanic Atmospheric Administration (NOAA). We also use the European Centre for Medium-Range Weather Forecasts (ECMWF) Atmospheric Reanalysis of the Twentieth Century (ERA20C) reanalysis dataset, which covers the period 1910–2010 at 2.5° × 2.5° spatial resolution (Poli et al. 2016).

(a)

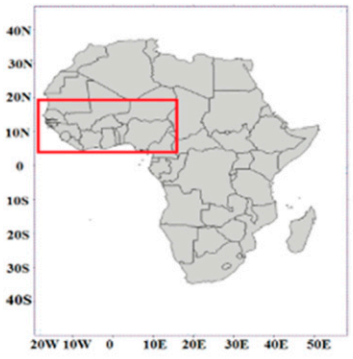

(b)

INPUTS (Daily Rainfall and Daily Temperature)

Datasets	Period	Resolution	References
20CR	1910-2009	2.5°x2.5°	Compo et al., 2011
NCEP	1948-2017	2.5°x2.5°	Kalnay et al., 1996
ERA20C	1910-2009	2.5°x2.5°	Uppala et al., 2005

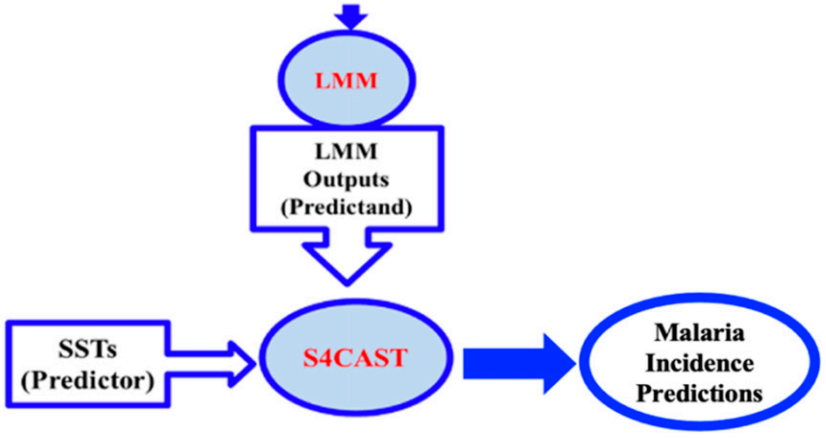

FIG. 1. (a) Location of the study area: West Africa (4°–18°N and 0°–15°E) is outlined in red; (b) chart showing the different reanalysis datasets used to simulate malaria incidence with the LMM, together with their full time periods, spatial resolutions, and associated references, up to the step of driving the S4CAST model from the SSTs (predictors) and the LMM outputs (predictand). The malaria incidence data used as a predictand are simulated malaria incidence by the LMM, fed by daily rainfall and temperature data of the reanalysis datasets.

The validation is performed with observed anomalies of malaria incidence from different West African countries. These observations are obtained from the Global Health Data Exchange (GHDx) project (http://ghdx.healthdata.org/gbd-results-tool), which synthesizes numerous input sources to estimate mortality, causes of death and illness, and risk factors for diverse diseases.

The SST monthly mean data are derived from the Extended Reconstructed SST database, version 3b (ERSST V3b), with a spatial resolution of 2.0° × 2.0° spanning January 1854 to May 2015 (Smith and Reynolds 2003, 2004; Smith et al. 2008). The three key SST regions (see Fig. S1 in the online supplemental material) known to affect the West African climate are examined: (i) the tropical Atlantic region (TA; 30°S–10°N, 30°W–10°E), (ii) the tropical Pacific area (TP; 30°S–20°N, 150°–90°W), and (iii) the Mediterranean region (MED; 30°–43°N, 10°W–43°E). Monthly anomalous SST indices are calculated for the indicated ocean regions. The availability of the reanalysis data determines the reference period.

b. Method

We use the LMM driven by different climate reanalysis over West Africa. The LMM is a mathematical–biological model for malaria transmission based on the impact of surface air temperatures and rainfall variability on the development cycles of the malaria vector in its larval and adult stage and of the parasite

and human host. The components of the LMM and the parameter settings are described in Hoshen and Morse (2004) and Ermert et al. (2011). To summarize, the number of emerging adult mosquitoes at the beginning of each month depends on the rain falling during the previous month. The mosquito population is then combined with the biting rate, sporogonic cycle length, and survival probability calculated from temperatures and the other parameters provided as input to the model. The LMM model has been successfully validated against a clinical record in Botswana (Jones and Morse 2010) and Senegal (Diouf et al. 2017). In this study, the standard parameter setting for malaria transmission is used.

The SST indices are calculated in terms of area averages of the anomalies over the TA, TP, and MED regions for different monthly lags with respect to an index of simulated malaria incidence (%) calculated for West Africa (4°–18°N, 20°W–15°E) to determine the seasons showing the higher correlation coefficients (see Fig. 2). We consider monthly lag 0–lag 5, where lag 0 corresponds to synchronous correlations between simulated malaria incidence and SST indices in September–November (SON). In contrast, lag 5 corresponds to correlations between SST indices in April–June (AMJ) and malaria indices in SON. We use the 20CR-driven malaria simulations (LMM incidence outputs) as they are available over the longest period and can provide an initial assessment of the seasons to be considered. A figure highlighting the seasonality of rainfall, temperature, and malaria incidence is provided as online supplemental material (Fig. S2 in the online supplemental material). We consider the SON season for malaria incidence since it has been shown as the period with the largest number of observed malaria cases over West Africa (Diouf et al. 2020). The same season is used for temperature because of its peak coinciding with the malaria season.

For rainfall, we focus on July–September (JAS), which represents the monsoon peak season. In a second step, we quantify the association between SST variability in the TA, TP, and MED regions and anomalous simulated malaria incidence for the SON transmission season. We use the S4CAST tool (Suárez-Moreno and Rodríguez-Fonseca 2015) to study these relationships, which is based on maximum covariance analysis (MCA). The MCA is a broadly used statistical discriminant analysis method to calculate principal directions of maximum covariance between two variables (e.g., Wallace and Gutzler 1981; von Storch and Zwiers 2001). This statistical analysis considers two fields, **Y** (predictor) and **Z** (predictand), for applying the singular value decomposition (SVD) to the cross-covariance matrix **C** between **Y** and **Z** to maximize it. The SVD is an algebraic technique to diagonalize nonsquare matrices, like the covariance matrix of two fields with different sizes (von Storch and Frankignoul 1998).

The S4CAST performs cross-validated hindcasts following the leave-one-out method (Dayan et al. 2014). This method is intended as a model validation technique. In the first step, data for the predictor and the predictand fields are removed for a given time step (i.e., a given year). Next, the MCA is applied with the remaining data to calculate the regression coefficients. Third, the regression coefficients and predictor data (previously removed) are used to estimate the cross-validated hindcast. Once the cross-validated hindcasts are obtained for the whole time series, the skill score of the model is assessed by calculating the Pearson correlation coefficients between the original (removed) data to be predicted and the generated hindcasts. Extended details of the application of MCA to analyze the SST-forced atmospheric teleconnections with the Sahel can be found in Suárez-Moreno et al. (2018).

The S4CAST is herein applied to the covariance matrix calculated between SST anomalies corresponding to each ocean predictor (TP, TA, and MED) and simulated malaria incidence over West Africa. We focus on the first (leading) MCA modes, which explain the highest percentage of explained covariance, the so-called squared covariance fraction (scf). These modes exhibit periods of significant correlation (SC) between the expansion coefficients time series of SST (U; predictor) and malaria incidence (V; predictand) calculated in terms of 21-yr running correlation windows. The existence of SC and nonsignificant correlation (NSC) periods indicates the potential nonstationary (i.e., changing) behavior of SST-forced teleconnections. The SC periods represent intervals for which covariability modes are typically more robust along a given sequence of decades (Suárez-Moreno and Rodríguez-Fonseca 2015; Suárez-Moreno et al. 2018). In contrast, associations are generally weaker for periods showing NSC. TheS4CAST uses the nonparametric Monte Carlo method under several user selectable random permutations to assess statistical significance. In this study, we set the 90% significance level under 500 permutations.

Further analysis based on S4CAST outputs is carried out using composite maps calculated from the SST expansion coefficient U associated with the SST–malaria incidence leading MCA modes. These maps focus on the 20CR experiment and are computed as mean anomalies for high minus low events, corresponding to values above 1 positive and below 1 negative standard deviation (hereinafter std) of the SST expansion coefficients, respectively.

For simplicity, we show the patterns corresponding to a particular phase of the modes. The opposite patterns must be considered for negative loadings of the expansion coefficients due to the linearity of the MCA method. A specific section is dedicated to the validation, or our results derived from the use of LMM to generate malaria incidence (section 4). In this regard we compute a correlation map between an index of observed malaria incidence (GHDx) for 1990–2009 (20 years) and global anomalous SSTs in July. This map is compared with additional simulations with the S4CAST tool using the LMM outputs based on the 20CR reanalysis as predictand fields but for the analysis period 1990–2009 to be consistent with GHDx data availability. The SST predictors are the same as described in section 2a (TA, TP, and MED), with an extra simulation in which the predictor encompasses the western tropical Pacific.

3. Results

a. *Relationship between SST indices and malaria incidence*

Figure 2 shows 21-yr running correlation windows between simulated malaria incidence over West Africa (20CR) and the different SST indices at different monthly lags. Overall, periods of significant correlation between SST predictors and

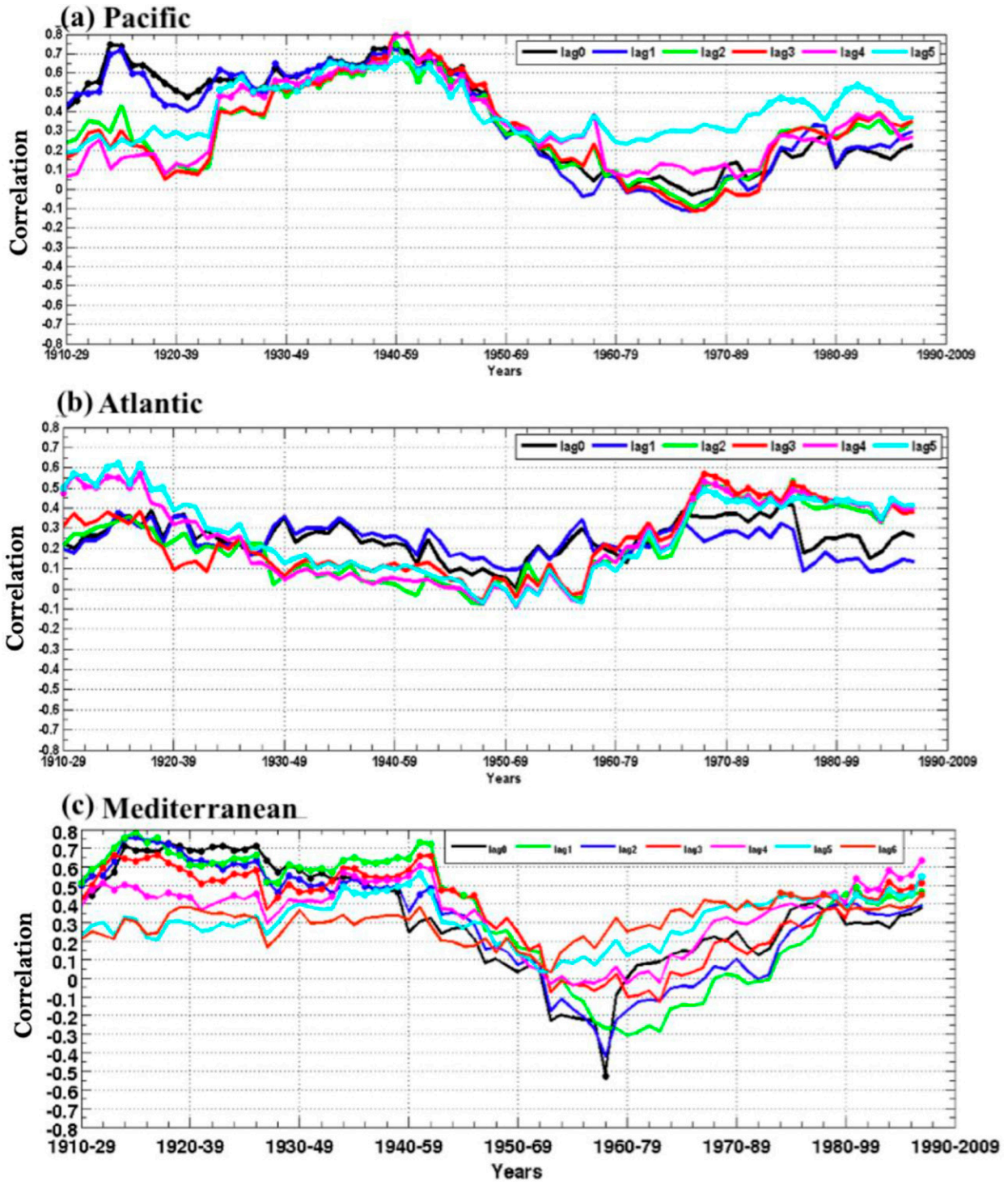

FIG. 2. The 21-yr sliding window correlation (1910–2009) between an index of anomalous malaria incidence in West Africa (4°–18°N, 20°W–15°E) for SON simulated with the LMM and the indices of anomalous SST. Results are shown corresponding to the SST indices calculated for the (a) eastern TP (30°S–20°N, 150°–90°W); (b) TA (30°S–10°N, 30°W–10°E); and (c) MED (30°–42°N, 10°W–42°E). The SST indices are computed for monthly lag 0 (SON), lag 1 (August–October), lag 2 (JAS), lag 3 (June–August), lag 4 (May–July), and lag 5 (AMJ). The sliding window correlation for each monthly lag is displayed according to different colored lines (see the legend in the panels). The dots indicate statistical significance of the correlation at the 90% level under nonparametric Monte Carlo testing (500 random permutations).

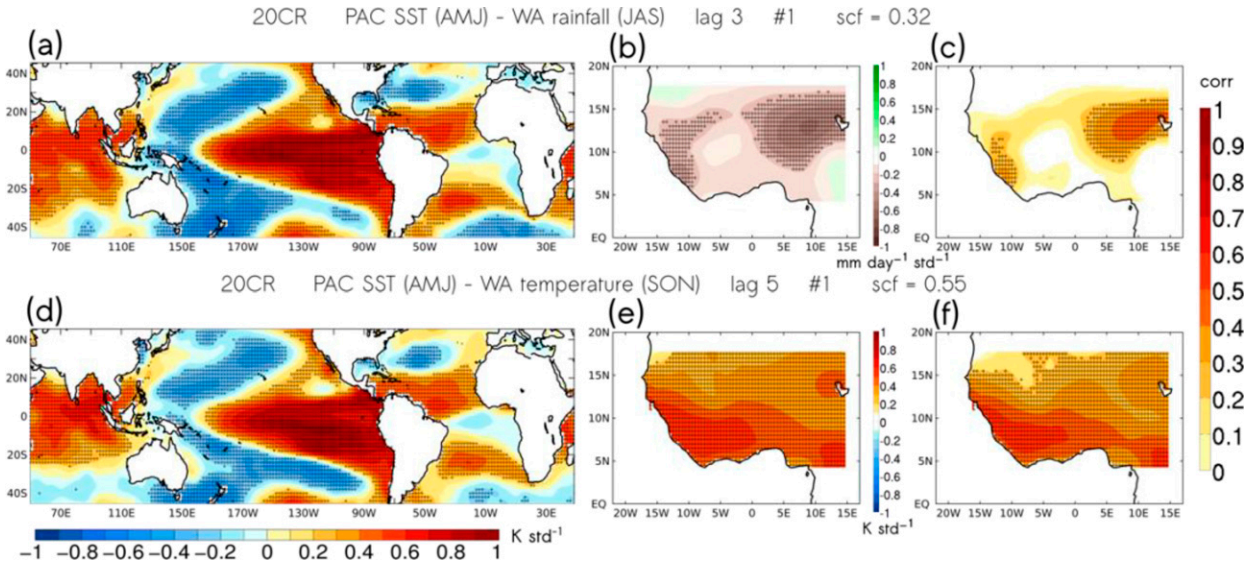

FIG. 3. Regression maps and correlation skill scores associated with the leading (top) SST(AMJ)–rainfall(JAS) and (bottom) SST(AMJ)-T2m(SON) MCA modes using the 20CR reanalysis. (a) Homogeneous SST (K std^{-1}) regression map calculated by regression of the SST expansion coefficient U (not shown) associated with the leading SST–rainfall MCA mode onto anomalous SST in the TP region (150°–90°W, 30°S–20°N). (b) Heterogeneous rainfall (mm day^{-1} std^{-1}) regression map calculated by regression of U (not shown) associated with the leading SST–rainfall MCA mode onto anomalous rainfall in West Africa (20°W–15°E, 4°–18°N). (c) Correlation skill scores calculated between observations and cross-validated hindcasts of rainfall associated with the leading SST–rainfall MCA mode. (d) Homogeneous SST (K std^{-1}) regression map calculated by regression of U (not shown) associated with the leading SST–T2m MCA mode onto anomalous SST in the TP region. (e) Heterogeneous T2m (K std^{-1}) regression map calculated by regression of U (not shown) associated with the leading SST–T2m MCA mode onto anomalous T2m in the Sahel. (f) Correlation skill scores calculated between observations and cross-validated hindcasts of T2m associated with the leading SST–T2m MCA mode. The scf for the leading MCA modes is indicated above the plots. Stippling denotes statistical significance at the 90% level based on nonparametric Monte Carlo testing (500 random permutations).

malaria incidence are found during the first half of the twentieth century and from 1980 to 1990 for all oceanic basins (Figs. 2a–c). The correlation curve presents two periods of SC from 1910 to 1940 and from 1980 up to 2009, while no significant correlation is found in the period in between. SC periods are observed up to monthly lag 5 corresponding to the AMJ season for the oceanic predictors, indicating potential predictability of anomalous malaria incidence up to 5 months in advance (in SON). Therefore, the application of the S4CAST model focuses on studying the predictability of the simulated malaria incidence in SON using the SST predictors in AMJ as a potential source of seasonal predictability.

b. *Covariability modes and prediction skill for the tropical Pacific*

Figure 3 shows the regression maps associated with the leading MCA mode for the TP SST predictor. The covariability modes between SST and climatic inputs (20CR rainfall and temperature) depict a positive ENSO-like pattern (El Niño; Figs. 3a–d) related to decreased rainfall in JAS (Fig. 3b) and increased temperatures in SON (Fig. 3e). In both cases, the significant responses are associated with significant correlation skill scores (Figs. 3c–f), denoting the robustness of the signals. Similar calculations based on other datasets (NCEP and ERA20C, Fig. S3 in the online supplemental material) indicate that the results are consistent with 20CR for the same periods.

In Fig. 4a, warm ENO-like SST anomalies (El Niño pattern) are associated with negative malaria incidence (Fig. 4b). Consistent results are found for the same periods when using other reanalysis products as inputs (NCEP and ERA20C) (Fig. S3).

The forecast skill scores as provided by the S4CAST model (Fig. 4a) depict regions of significant positive correlations. However, differences are shown depending on the reanalysis used to generate the time series of malaria incidence, with positive correlations scattered in the Sahelian part of West Africa.

c. *Covariability modes and prediction skill for the tropical Atlantic*

For the TA region, the SST patterns associated with the leading MCA modes depict a positive AEM-like pattern related to positive rainfall anomalies over southern West Africa and negative anomalies over northern West Africa (Figs. 5a,b), and widespread positive surface air temperature (T2m) anomalies (Figs. 5d,e). Positive and significant correlation skill scores highlight the robustness of the response signals (Figs. 5c,d).

For the malaria incidence (Fig. 6), a tropical SST warming that resembles the positive AEM phase (Fig. 6a) is associated with negative anomalies over the Sahel and positive anomalies over the Gulf of Guinea (Fig. 5b). The signal over the Sahel is significant for the 20CR (Fig. 5b) and NCEP experiments (Fig. S4 in the online supplemental material). Such

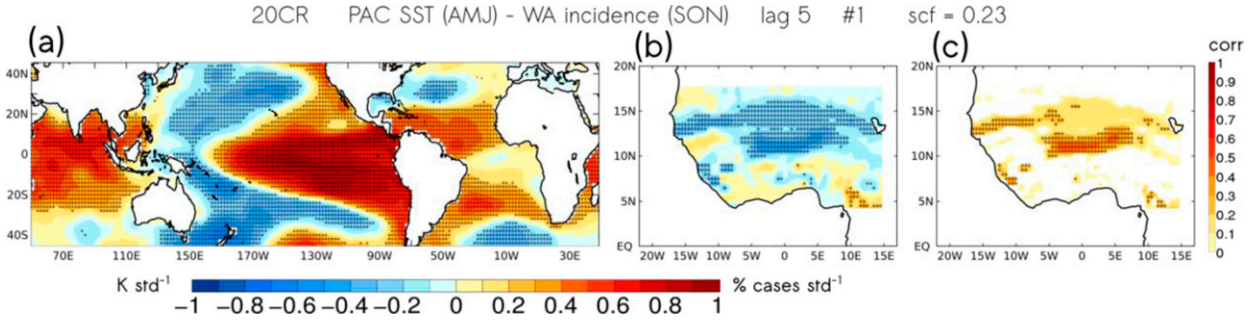

FIG. 4. Regression maps and correlation skill scores associated with the leading SST(AMJ)–malaria incidence(SON) MCA modes using the 20CR reanalysis. (a) Homogeneous SST (K std^{-1}) regression map calculated by regression of U (not shown) associated with the leading SST–malaria incidence MCA mode onto anomalous SST in the TP region (150°–90°W, 30°S–20°N). (b) Heterogeneous malaria incidence (% cases std^{-1}) regression map calculated by regression of U (not shown) associated with the leading SST–rainfall MCA mode onto anomalous malaria incidence in West Africa (20°W–15°E, 4°–18°N). (c) Correlation skill scores calculated between simulated malaria incidence with the LMM model and cross-validated hindcasts of malaria incidence associated with the leading SST–malaria incidence MCA mode. The scf is indicated above the plots. Stippling denotes statistical significance at the 90% level based on nonparametric Monte Carlo testing (500 random permutations).

similar responses of malaria incidence for the three different reanalysis datasets suggest the SST-forced response of malaria incidence to be statistically stationary throughout the study period. Overall, positive significant correlation skill scores are located over the western Sahel and local areas in the southern region of the Gulf of Guinea (Fig. 6c).

d. *Covariability modes and prediction skill for the Mediterranean*

Widespread positive rainfall anomalies characterize the impact of warm MED SST anomalies in West African during JAS (Fig. 7b). These positive SST anomalies are associated

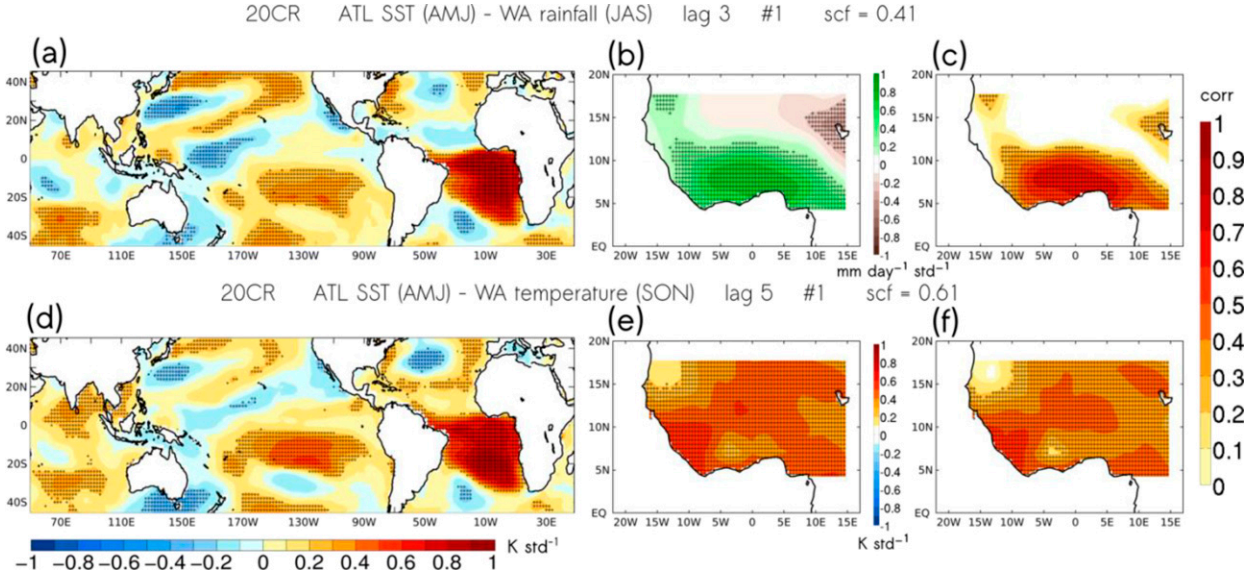

FIG. 5. Regression maps and correlation skill scores associated with the leading (top) SST(AMJ)–rainfall(JAS) and (bottom) SST(AMJ)–T2m(SON) MCA modes using the 20CR reanalysis. (a) Homogeneous SST (K std^{-1}) regression map calculated by regression of U (not shown) associated with the leading SST–rainfall MCA mode onto anomalous SST in the TA region (30°W–10°E, 30°S–10°N). (b) Heterogeneous rainfall (mm day^{-1} std^{-1}) regression map calculated by regression of U (not shown) associated with the leading SST–rainfall MCA mode onto anomalous rainfall in West Africa (20°W–15°E, 4°–18°N). (c) Correlation skill scores calculated between observations and cross-validated hindcasts of rainfall associated with the leading SST–rainfall MCA mode. (d) Homogeneous SST (K std^{-1}) regression map calculated by regression of U (not shown) associated with the leading SST–T2m MCA mode onto anomalous SST in the TA region. (e) Heterogeneous T2m (K std^{-1}) regression map calculated by regression of U (not shown) associated with the leading SST–T2m MCA mode onto anomalous T2m in the Sahel. (f) Correlation skill scores calculated between observations and cross-validated hindcasts of T2m associated with the leading SST–T2m MCA mode. The scf for the leading MCA modes is indicated above the plots. Stippling denotes statistical significance at the 90% level based on nonparametric Monte Carlo testing (500 random permutations).

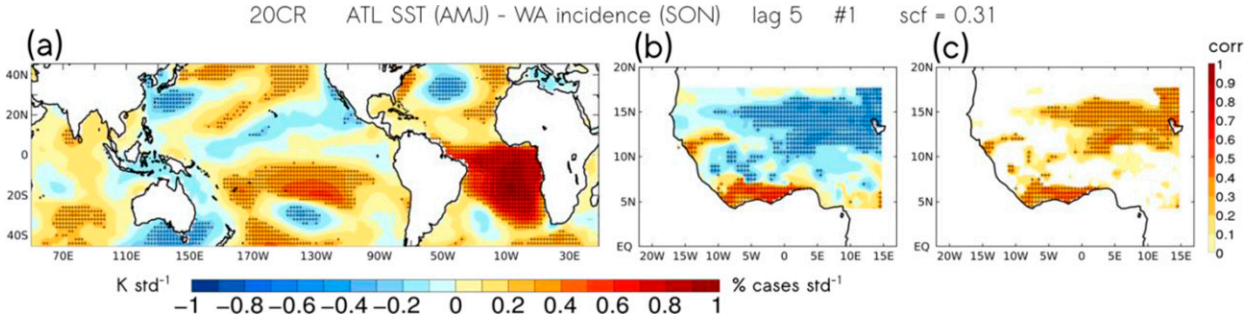

FIG. 6. Regression maps and correlation skill scores associated with the leading SST(AMJ)–malaria incidence(SON) MCA modes using the 20CR reanalysis. (a) Homogeneous SST (K std^{-1}) regression map calculated by regression of U (not shown) associated with the leading SST–malaria incidence MCA mode onto anomalous SST in the Atlantic region (30°W–10°E, 30°S–10°N). (b) Heterogeneous malaria incidence (% cases std^{-1}) regression map calculated by regression of U (not shown) associated with the leading SST–rainfall MCA mode onto anomalous malaria incidence in West Africa (20°W–15°E, 4°–18°N). (c) Correlation skill scores calculated between simulated malaria incidence with the LMM model and cross-validated hindcasts of malaria incidence associated with the leading SST–malaria incidence MCA mode. The scf is indicated above the plots. Stippling denotes statistical significance at the 90% level based on nonparametric Monte Carlo testing (500 random permutations).

with decreased SON temperatures over the western half of West Africa (Fig. 7e).

An increase in malaria incidence over the Sahel is shown in response to positive SST anomalies (Fig. 8a). The 20CR (Fig. 8) and NCEP (lower panels of Fig. S5 in the online supplemental material) experiments show similar results, while ERA20C experiments show positive anomalous SSTs associated with decreased malaria incidence over the Sahel (Fig. S5, upper panels). Correlation skill scores in predicting precipitation anomalies (Fig. 7c), and a significant T2m signal restricted to the

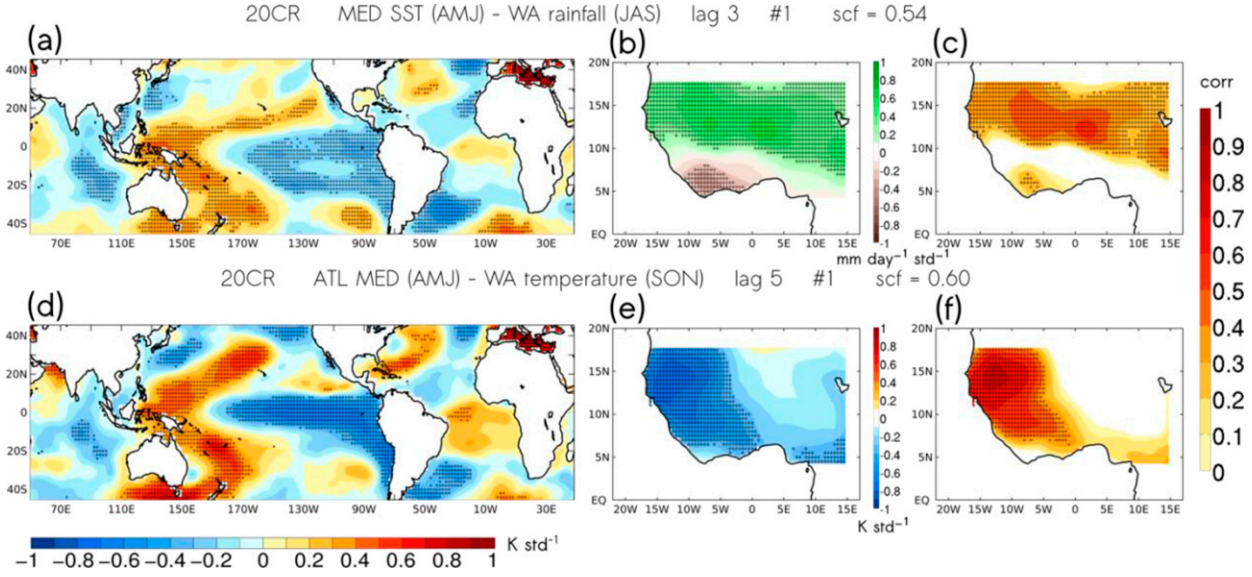

FIG. 7. Regression maps and correlation skill scores associated with the leading (top) SST(AMJ)–rainfall(JAS) and (bottom) SST(AMJ)–T2m(SON) MCA modes using the 20CR reanalysis. (a) Homogeneous SST (K std^{-1}) regression map calculated by regression of U (not shown) associated with the leading SST–rainfall MCA mode onto anomalous SST in the Mediterranean region (10°W–42°E, 30°–42°N). (b) Heterogeneous rainfall (mm day^{-1} std^{-1}) regression map calculated by regression of U (not shown) associated with the leading SST–rainfall MCA mode onto anomalous rainfall in West Africa (20°W–15°E, 4°–18°N). (c) Correlation skill scores calculated between observations and cross-validated hindcasts of rainfall associated with the leading SST–rainfall MCA mode. (d) Homogeneous SST (K std^{-1}) regression map calculated by regression of U (not shown) associated with the leading SST–T2m MCA mode onto anomalous SST in the Mediterranean region. (e) Heterogeneous T2m (K std^{-1}) regression map calculated by regression of U (not shown) associated with the leading SST–T2m MCA mode onto anomalous T2m in the Sahel. (f) Correlation skill scores calculated between observations and cross-validated hindcasts of T2m associated with the leading SST–T2m MCA mode. The scf for the leading MCA modes is indicated above the plots. Stippling denotes statistical significance at the 90% level based on nonparametric Monte Carlo testing (500 random permutations).

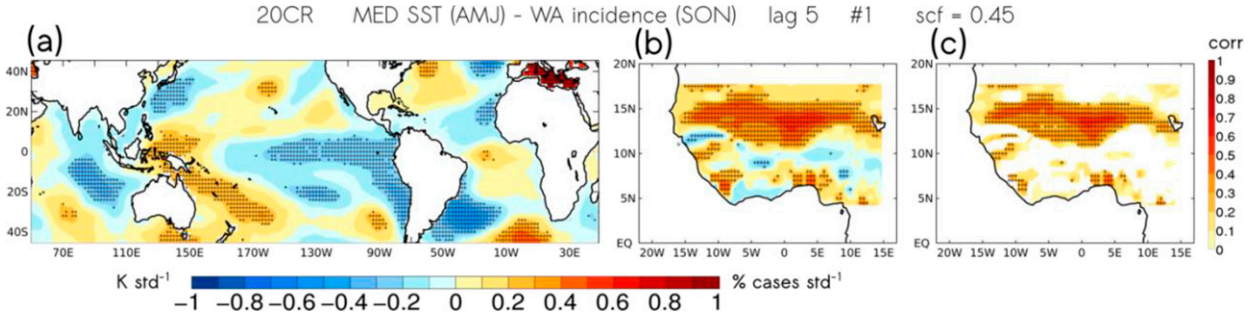

FIG. 8. Regression maps and correlation skill scores associated with the leading SST(AMJ)–malaria incidence(SON) MCA modes using the 20CR reanalysis. (a) Homogeneous SST (K std^{-1}) regression map calculated by regression of U (not shown) associated with the leading SST–malaria incidence MCA mode onto anomalous SST in the Mediterranean region (10°W–42°E, 30°–42°N). (b) Heterogeneous malaria incidence (% cases std^{-1}) regression map calculated by regression of U (not shown) associated with the leading SST–rainfall MCA mode onto anomalous malaria incidence in West Africa (20°W–15°E, 4°–18°N). (c) Correlation skill scores calculated between simulated malaria incidence with the LMM model and cross-validated hindcasts of malaria incidence associated with the leading SST–malaria incidence MCA mode. The scf is indicated above the plots. Stippling denotes statistical significance at the 90% level based on nonparametric Monte Carlo testing (500 random permutations).

western part of the region (Fig. 7f), closely matches the significant skill scores in reproducing simulated malaria incidence that is mainly constrained to the Sahel (Fig. 8c).

e. *Comparison of skill scores between climate variables and malaria incidence*

We aim to compare the climate-related skill scores (Fig. 3, left panel; Fig. 5, left panel; Fig. 7, left panel) with those derived from simulating malaria incidence (Figs. 4c, 6c, and 8c). Negative malaria incidence anomalies are shown over West Africa (Fig. 4b) as a response to warmer TP SST conditions (Fig. 4a). This signal is consistent with the decrease in rainfall (Fig. 3b) and warmer T2m (Fig. 3e). Figure 3 also shows the skill in predicting rainfall and temperature based on SST predictors (Figs. 3c,f). Focusing on 20CR reanalysis (Fig. 4c), TP SST anomalies are shown as a skillful predictor of malaria incidence over Sahelian longitudes ranging between 5°W and 5°E. This significant malaria incidence response does not entirely correspond to the significant rainfall signal over the eastern part of West Africa (Fig. 3c). For T2m, the significant signal encompasses the whole study region (Figs. 3e, 5e and 7e). Based on these findings, we suggest the potential nonlinear interaction between rainfall and T2m anomalies as a modulator of simulated malaria incidence.

For the TA SST predictor, positive rainfall anomalies over most parts of West Africa (except for the northeastern part where negative rainfall anomalies are located) tend to favor an increase in malaria incidence over the Gulf of Guinea (Fig. 5b). The malaria incidence decreases over the Sahel under the same (opposite) SST anomalies (Fig. 6b). Figures 5c–f show the skill scores to reproduce rainfall and T2m variability based on TA SST anomalies. Generalized significant skill scores are found for T2m, while the rainfall signal is constrained to the southern half of the study region. When comparing the skill scores found for T2m (Fig. 5f) and malaria incidence using the 20CR reanalysis data (Fig. 6c), significant signals are depicted in both south and northeast regions.

As for MED SST anomalies, significant skill scores are shown to reproduce precipitation anomalies (Fig. 7c), whereas a significant T2m signal is restricted to the western part of the region (Fig. 7f). These signals closely match the significant skill scores in simulating malaria incidence over the Sahel (Fig. 8c).

To further explore this relationship, we apply the S4CAST model to calculate the leading MCA modes between SST anomalies in the eastern tropical Pacific in AMJ (predictor field) and two different anomalous fields to be predicted. The first one corresponds to West African rainfall anomalies during JAS. The second field corresponds to T2m during SON. Composite maps based on the 20CR reanalysis shows that the El Niño signal is associated with anomalous upward movements of air (reflected by positive anomalies of the velocity potential at 200 hPa on), which in turn affects the zonal Walker circulation resulting in anomalous air subsidence (drier conditions) over West Africa (Figs. S6b,c in the online supplemental material). This subsidence is concomitant with negative rainfall anomalies and is consistent with the results shown in Fig. 3a. Nonsignificant and weak T2m anomalies over West African do not affect the climatological surface temperatures (Fig. 6d), which range from 26° to 34°C following a meridional gradient to the north. Under this scenario, the underlying negative rainfall anomalies (Fig. 3a) do not favor an increase in incidence during the subsequent malaria season (SON), even though surface temperatures may be favorable in certain regions, notably in the southern part of the Gulf of Guinea where temperatures are around 27°C. A significant decrease in simulated malaria incidence farther north (Fig. 4a) is concomitant with temperatures exceeding 32°C. This threshold is close to the optimal temperature values for malaria transmission.

Warmer SST anomalies in the tropical Atlantic lead to a southward shift of the ITCZ in response to a positive gradient of anomalous sea level pressure (SLP) to the south, reducing and increasing rainfall in the northern and southern West

African regions, respectively. This is consistent with the composite map based on the SST expansion coefficient (Fig. S7a in the online supplemental material) associated with the leading SST–malaria incidence MCA mode shown (see Fig. 6). Indeed, the SLP anomaly pattern depicts a positive gradient to the south (Fig. S7b) that reduces the northward shift of the ITCZ, increasing rainfall over the southern areas of West Africa while precipitation decreases over the Sahel. This result is consistent with the so-called West African rainfall dipole in response to the AEM (e.g., Losada et al. 2010b). As for T2m, composite maps reveal significant negative anomalies over the whole study region except for a positive signal north of Senegal (Fig. S7c). These anomalies place the T2m climatological range between 24° and 27°C to the south (Fig. S7d), combined with positive rainfall anomalies to increase malaria incidence. By contrast, drier conditions reduce malaria incidence to the north. It follows that malaria incidence decreases over the Sahel and increases over equatorial latitudes, in agreement with Fig. 6b.

As stated, the leading MCA mode between MED SST anomalies and malaria incidence for the 20CR reanalysis (is characterized by a MED SST warming related to an increase of malaria incidence that affects the Sahelian part of West Africa (see Fig. 8). The same analysis is applied for the MED predictor in terms of composite maps based on the MED SST expansion coefficient (Fig. S8a in the online supplemental material). A longitudinal band of specific humidity anomalies at 850 hPa is located over the Sahel in response to low-level moisture transport to the south, feeding moisture convergence due to warmer Mediterranean SST in JAS (Fig. S8b). T2m increases following the monsoon season, resulting in positive anomalies over the central and eastern Sahel during the subsequent SON season (Fig. S8c). These T2m anomalies are responsible for absolute values of surface temperatures (Fig. S8d) that, combined with positive rainfall anomalies (see Fig. 7b), favor the increase of malaria incidence in the West African Sahel (Fig. 8b).

Further analysis is based on the time-varying relationship between SST predictors and predictand fields (i.e., anomalies of malaria incidence, rainfall, and temperature). In this context, sliding windows correlation between the time series expansion coefficients derived from the leading MCA modes for the TP predictor denotes a similar evolution for T2mand rainfall, with the SC periods closely pairing. The signal corresponding to simulated malaria incidence also follows an analogous behavior (Fig. S9a in the online supplemental material). The same calculations applied to the TA SST predictor (Fig. S9b) depict similar time-varying signals for the three predictand fields, even though the link is more robust for T2m as shown in terms of higher significant correlations. Likewise, the signals associated with the MED SST predictor are very similar for the three predictand fields (Fig. S9c). The similarity of the time series presented in this section for each SST predictor, showing SC periods for which the spatial covariability patterns associated with the different predictand fields closely coincide, makes the results derived from this study more consistent.

4. Validation of SST–malaria relationship

This section presents a validation of our results based on the SST-forced response of malaria incidence. To this aim, we focus on the 1990–2009 period for which observations of malaria incidence obtained from the GHDx project (see section 2a for extended details) are available beyond the simulated malaria incidence with the LMM. These observations are used to create an index of malaria incidence calculated as an average for the Sahelian countries (Burkina Faso, Mali, Senegal, Niger, and Mauritania).

First, the leading MCA modes are calculated between SST anomalies and anomalous malaria incidence (LMM output) as previously done for the three ocean predictors with the S4CAST model (see Figs. 4, 6, and 8 for TP, TA, and MED, respectively), but for the study period 1990–2009 (Fig. 9). For the eastern and western TP SST predictors (Figs. 9a–c and 9d–f, respectively), the results approach the leading MCA mode previously calculated and its associated cross-validated skill scores (cf. Fig. 4), which exhibits a positive ENSO-like SST pattern related to decreased malaria incidence over the Sahel. This similarity is because the study range (1990–2009) falls within the Pacific SC period (see Fig. S9a in the online supplemental material; red line). During this validation period, the interbasin connection between the equatorial Atlantic and Pacific (Rodríguez-Fonseca et al. 2009) could synergistically enhance malaria's impact. In the case of the TA SST predictor (Figs. 9g–i), the spatial patterns for both SST anomalies and anomalous malaria incidence differ significantly from the MCA modes corresponding to the SC period (cf. Fig. 6). Contrary to the previous case, this is attributed to the interval 1990–2009 not belonging to the SC Atlantic period (see Fig. S9b; red line). For the MED SST predictor, the spatial patterns derived from MCA analysis for the 1990–2009 interval (Figs. 9j–l) closely reproduce the covariability patterns corresponding to the SC period (cf. Fig. 8). Note that the MED SC period encompasses the shorter 1990–2009 study interval (see Fig. S9c; red line).

Next, the index of observed malaria incidence is correlated with global SST anomalies (Fig. 9m). Significant opposing signals are shown over the tropical Pacific and Atlantic basins, with the Pacific (Atlantic) SST anomalies correlating negatively (positively) with the index of observed malaria incidence. This is consistent with a Pacific–Atlantic counteracting SST effect associated with a significant response of malaria incidence in the Sahel (see Figs. 9a–i). Indeed, this counteracting effect has been previously highlighted by its strong impact on rainfall variability in the West African Sahel (Rodríguez-Fonseca et al. 2011; Losada et al. 2012; Suárez-Moreno et al. 2018). For the Mediterranean SST variability, no significant correlations are found, suggesting that the Pacific–Atlantic counteracting effect prevails over the Mediterranean influence. Under this scenario, significant SST anomalies in the Mediterranean Sea represent a source of predictability of malaria incidence when the tropical Pacific and Atlantic basins lack significant anomalies. A summary table with the influence of each SST predictor on the variability of malaria

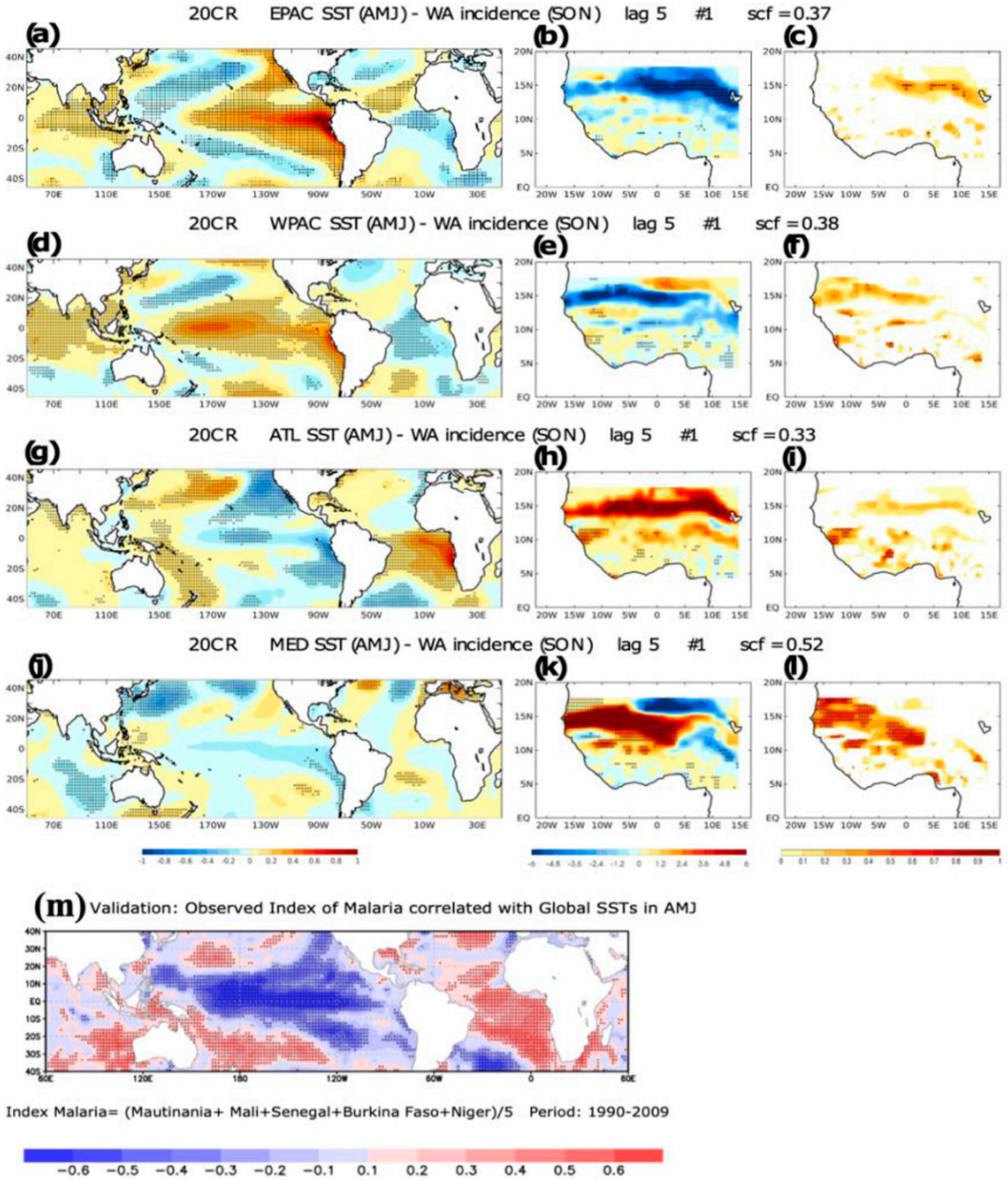

FIG. 9. Regression maps and correlation skill scores associated with the leading SST(AMJ)–malaria incidence(SON) MCA modes using the 20CR reanalysis for the period 1990–2009. Homogeneous SST (K std^{-1}) regression map calculated by regression of the SST expansion coefficient associated with the leading SST–malaria incidence MCA mode onto anomalous SST in the (a) eastern Pacific (EPAC; 150°–90°W, 30°S–20°N), (d) western Pacific (WPAC; 160°E–150°W, 20°S–10°N), (g) Atlantic region (30°W–10°E, 30°S–10°N) and (j) Mediterranean region (10°W–42°E, 30°–42°N). (b),(e),(h),(k) Heterogeneous malaria incidence (% cases std^{-1}) regression map calculated by regression of the SST expansion coefficient associated with the leading SST–rainfall MCA mode onto anomalous malaria incidence in West Africa (20°W–15°E, 4°–18°N). (c),(f),(i),(l) Correlation skill scores calculated between simulated malaria incidence with the LMM model and cross-validated hindcasts of malaria incidence associated with the leading SST–malaria incidence MCA mode. The scf is indicated above the plots. Stippling denotes statistical significance at the 90% level based on nonparametric Monte Carlo testing (500 random permutations). (m) Correlation maps of the GHDx incidence anomalies observe in the period 1990–2009 (20 years) and the anomalous SSTs in July of the year of the incidence.

incidence in West Africa is provided in the online supplemental material (Table S1).

5. Discussion and conclusions

Studies of the relationship between climate and malaria transmission in the sub-Saharan region of West Africa are of paramount importance. In this region, the spread of malaria appears to be endemic and relatively higher in comparison with other tropical areas, and knowledge of the consequences of climate variability and change are not available to the vulnerable population. Therefore, our study aims to eliminate this knowledge gap, helping to understand the link between malaria transmission and climate factors at a regional level by analyzing the role of potential SST predictors in driving malaria outbreaks.

We used the S4CAST model (Suárez-Moreno and Rodríguez-Fonseca 2015) to evaluate the predictability of malaria incidence motivated by two main reasons. On the one hand, SST variability in the tropical Pacific and Atlantic basins and the Mediterranean Sea is known to exert a strong influence on the West African monsoon dynamics (e.g., Fontaine et al. 1998; Nicholson and Grist 2001; Rowell 2013; Giannini et al. 2020, among others), which in turn directly or indirectly impacts other essential sectors including agriculture and the seasonal occurrence of vector-borne diseases in general, and malaria outbreaks in particular. On the other hand, the nonstationary (i.e., changing over time) influence of SSTs on West African rainfall has been reported in previous studies (Janicot et al. 1996, 1998; Ward 1998; Rodríguez-Fonseca et al. 2011; Mohino et al. 2011; Losada et al. 2012; Suárez-Moreno et al. 2018; Suárez-Moreno 2019). By extension, this nonstationary behavior would be responsible for changing impacts on other variables, such as the incidence of malaria known to be driven by climatic factors (Poveda et al. 2001; Diouf et al. 2017, 2020).

Our results demonstrate robust SST-forced atmospheric teleconnections driving the variability of surface air temperatures (T2m) and precipitation in West Africa, which in turn influence the variability of simulated malaria incidence. The underlying mechanisms associated with the covariability modes between anomalous malaria incidence and SST anomalies were studied and compared with previous works that focused on SST impacts on West African rainfall, illustrating how SST variability directly modulates rainfall and T2m and indirectly affects malaria epidemics.

For tropical Pacific SST anomalies, skillful predictability of malaria incidence is found 5 months in advance, as illustrated with significant correlation skill scores up to 0.6 over the Sahel. In regard of the tropical Atlantic, significant correlation skill scores at the 5-month lead time that approaches values of 0.8 highlights robust predictability of malaria incidence. About the impact of Mediterranean SST, widespread significant correlation skill scores also at 5-month lead time reach values of 0.8 mainly over the western Sahel and local areas in the southern part of the Gulf of Guinea.

For the atmospheric mechanisms for the tropical Pacific region, the teleconnection is explained by enhanced or weakened subsidence in response to SST warming or cooling, respectively, that disrupts the upper-level Walker circulation. Accordingly, for the warm phase of ENSO (El Niño events), enhanced subsidence over West Africa reduces rainfall and increases surface air temperatures (e.g., Rowell 2001; Suárez-Moreno et al. 2018). The opposite pattern occurs for the negative phase of ENSO (La Niña events). Note that changes in the spatial patterns are observed depending on the reanalysis used to generate malaria incidence with the LMM (Fig. S3 in the online supplemental material). On the side of the ERA20C-related experiment (Figs. S3a–c), both the SST and malaria incidence patterns are similar (Figs. S3a and b, respectively), even though the significant correlation skill scores are lower and limited to Senegal. When using the NCEP reanalysis (Figs. S3d–f), the weakening of the negative significant response over the Sahel is potentially due to the presence of negative SST anomalies in the equatorial Atlantic region (negative AEM phase) that tends to counteract the ENSO impact over the Sahel (see, e.g., Losada et al. 2012). These differences in the covariability patterns between the reanalysis used to generate malaria incidence with the LMM might be related to different observational data used in the assimilation schemes and the distinct periods covered by these reanalysis products.

In the Atlantic Ocean, warm SST anomalies associated with the positive AEM phase (Atlantic Niño) are responsible for a weak temperature and pressure gradient to the north. This causes a low differential land–ocean contrast that reduces the inland monsoon flow as the ITCZ keeps equatorward (e.g., Chiang et al. 2000). By linearity of the MCA method, cold SST anomalies result in a strong positive gradient to the north that shifts the ITCZ northward, displacing the monsoon rain belt over Sahelian latitudes. This teleconnection mechanism was inferred for the leading MCA mode associated with the use of 20CR reanalysis to generate malaria incidence with the LMM (see Fig. 6), the spatial patterns being closely similar in the case of producing malaria incidence from the ERA20C product (Figs. S4a–c in the online supplemental material). However, the result referring to the use of the NCEP reanalysis is significantly different (Figs. S4d–f). Significant SST anomalies in the eastern subtropical Atlantic could be responsible for reduced cross-equatorial SST gradient to the north, maintaining the ITCZ and therefore the monsoon flow over the Guinean Gulf region, where the SST-forced response of anomalous malaria incidence is more robust while it weakens over the Sahel.

For the Mediterranean Sea, the southward advection of anomalous low-level moisture due to warmer SST enhances the rainfall response over the Sahel, playing a potential role in driving the variability of simulated malaria incidence over the region, and prevailing over temperature forcings (e.g., Rowell 2003; Gaetani et al. 2010). These results are consistent with Suárez-Moreno et al. (2018), who found that increased northeasterly moisture transport from warmer Mediterranean SST feeds moisture convergence over West Africa for a specific sequence of decades (the 1950s and after the 1990s),

which coincide with our significant correlation period. Besides warmer Mediterranean SSTs that should imply increase rainfall leading to augmented malaria incidence, the North Atlantic Ocean (in front of the coast of Senegal) shows negative SST anomalies, which should lead to reduced malaria incidence. This is consistent with a counteracting effect between the SST forcing associated with the Mediterranean and subtropical North Atlantic Ocean regions, making the signal misleading for the ERA20C-related malaria incidence as compared with the results derived from 20CR and NCEP products. Differences when using other reanalyses to generate malaria incidence are potentially due to cooler North Atlantic SSTs in ERA20C (Fig. S5a in the online supplemental material) relative to the results derived from 20CR and NCEP reanalysis (Fig. 8a and Fig. S5d, respectively). The pronounced SST cooling over the northern tropical Atlantic reduces the positive meridional SST gradient to the north, limiting the northward shift of the ITCZ, which reduces low-level convergence and, therefore, precipitation in the Sahel. Moreover, tropical Pacific SST cooling is stronger for the 20CR and NCEP experiments as it extends farther west. As a result, the SST-forced response of malaria incidence is enhanced for 20CR and NCEP reanalysis (Fig. 8b and Fig. S5e, respectively), while it is reversed for the ERA20C product (Fig. S5b).

Given that the leading modes of covariability between SST anomalies and anomalous malaria incidence are shown to be more robust for some periods than for others, it follows that these nonstationary relationships are associated with the changing behavior of atmospheric teleconnections. In this context, our results show that the correlations between El Niño (positive phase of ENSO) and rainfall over the southern part of West Africa are weaker than those with Sahelian precipitation in July, in agreement with Barnston et al. (1996). As rainfall decreases in the Sahel, malaria incidence is reduced, even though this relationship is changing over time, consistent with previous studies. For instance, Folland et al. (1986), Ward (1992), and Ropelewski and Halpert (1987) found no significant relationship between ENSO and rainfall over the Sahel. Moreover, interdecadal rainfall variability in the West African Sahel is pronounced in a way that a harsh drought period in the 1980s and early 1990s was followed by positive precipitation anomalies from the mid-1990s onward (Barnston et al. 1996) to confirm an apparent recovery trend (Giannini et al. 2003; Nicholson 2005; Hagos and Cook 2008).

The validation carried out in section 4 supported our results based on simulated malaria incidence and its robust relationship with SST-forced climate variability in West Africa. Nevertheless, there are some limitations in our study. For the validation of the model predictions against observed incidence data, the quality of malaria-related observations is limited. Validating our results over a large spatial domain (West Africa) and the long-term is difficult because of the data accessibility and quality. In this framework, only partial validation was performed for the 1990–2009 period by computing the correlation maps between an averaged index of malaria incidence (GHDx) for a series of West African countries and the anomalous SSTs. By construction, applying MCA for such a short period is not optimal, although the results are mostly consistent with the analysis of the longest period for which simulated malaria incidence with the LMM was used, showing the counteracting Pacific–Atlantic SST forcing as the leading driver of malaria incidence in the Sahel, while the Mediterranean would become a key source of predictability when tropical SST anomalies are not significant. As further limitations of this study, even if the impact of climate is essential in the occurrence of malaria, our biological model (the LMM) does not consider critical nonclimatic factors such as socioeconomic factors and early and strong public health measures taken by local governments. The large-scale migration of populations from areas in which malaria is endemic into new areas will also play an essential role in the dynamics of the disease (World Health Organization 2017; Rodrigues et al. 2018).

This work is not yet fully implemented into operational practice, and it is time to evaluate its potential benefits, particularly after postprocessing with the S4CAST algorithm. This encourages malaria prediction diagnostics to be extended to the whole African continent. An in-depth analysis of the indirect influence of ocean conditions on malaria is needed to confirm that the same method can be developed elsewhere. Our study is expected to be helpful to decision-makers knowing that the essential factor in reducing the impact of an epidemic is a timely response in which effective control measures are undertaken as soon as the episode has been predicted using climate information. Otherwise, due to the lack of reliable, validated malaria for a sizable spatiotemporal scale, extending this study to the whole African continent and elsewhere is somewhat a big challenge.

To better understand the impact of air–sea interactions on malaria incidence, further studies are encouraged that include sensitivity experiments with GCMs by prescribing SST anomalies in the Pacific Ocean, Atlantic Ocean, and Mediterranean Sea basins. Accordingly, the obtained T2m and precipitation would be introduced in the malaria model (LMM) to better determine the malaria model's sensitivity to these SST patterns and induced climate variability over West Africa. Furthermore, in future work, we would like to validate the S4CAST model hindcasts with other observed malaria-related data.

Acknowledgments. NOAA funded this work as part of a Service Level Agreement between the National Weather Service and the Climate Program Office. We thank this program, a scholarship from which was awarded to author Diouf and allowed the achievement of this study. We also thank the Department of Meteorology, Faculty of Physics, at the Universidad Complutense de Madrid (UCM), which supported special issues, mainly during Diouf's past stay within the framework of the cooperation project VR 63/12 between LPAOSF-UCAD (Dakar) and UCM (Madrid). Diouf, together with Roberto Suárez-Moreno, assisted by Belén Rodríguez Fonseca and Malick Wade, performed the experimental activities and analyzed the data. Diouf drafted and wrote the initial version of the paper. Suárez-Moreno revised the final version to improve its readability. Wassila Thiaw, Abdoulaye Deme, Jacques-André Ndione, Amadou

Thierno Gaye, and Rodríguez Fonseca designed and supervised the study. Anta Diaw and Marie Khemesse Ngom Ndiaye gave advice and discussion related to the malaria context. Cyril Caminade and Andy Morse provided advice and discussion related to the LMM simulations and improved the draft. All authors discussed the results and helped to improve the paper. The authors declare that they have no conflicts of interest for this article.

REFERENCES

Arab, A., M. C. Jackson, and C. Kongoli, 2014: Modelling the effects of weather and climate on malaria distributions in West Africa. *Malar. J.*, **13**, 126, https://doi.org/10.1186/1475-2875-13-126.

Barnston, A. G., W. Thiaw, and V. Kumar, 1996: Long-lead forecasts of seasonal precipitation in Africa using CCA. *Wea. Forecasting*, **11**, 506–520, https://doi.org/10.1175/1520-0434(1996)011<0506:LLFOSP>2.0.CO;2.

Bayoh, M. N., 2001: Studies on the development and survival of *Anopheles gambiae* sensu stricto at various temperatures and relative humidities. Ph.D. dissertation, Durham University, 151 pp., http://etheses.dur.ac.uk/4952/.

Bouma, M. J., and C. Dye, 1997: Cycles of malaria associated with El Niño in Venezuela. *J. Amer. Med. Assoc.*, **278**, 1772–1774, https://doi.org/10.1001/jama.1997.03550210070041.

——, G. Poveda, W. Rojas, D. Chavasse, M. Quinones, J. Cox, and J. Patz, 1997: Predicting high-risk years for malaria in Colombia using parameters of El Niño Southern Oscillation. *Trop. Med. Int. Health*, **2**, 1122–1127, https://doi.org/10.1046/j.1365-3156.1997.d01-210.x.

Breman, J. G., M.S. Alilio, and A. Mills, 2004: Conquering the intolerable burden of malaria: What's new, what's needed: A summary. *Amer. J. Trop. Med. Hyg.*, **71** (2_Suppl.), 1–15, https://doi.org/10.4269/ajtmh.2004.71.2_suppl.0700001.

Carnevale, P., V. Robert, J. F. Molez, and D. Baudon, 1984: Epidémiologie énérale: Faciès épidémiologiques des paludismes en Afrique subsaharienne. *Étud. Méd.*, **3**, 123–133.

Chiang, J. C. H., Y. Kushnir, and S. E. Zebiak, 2000: Interdecadal changes in eastern Pacific ITCZ variability and its influence on the Atlantic ITCZ. *Geophys. Res. Lett.*, **27**, 3687–3690, https://doi.org/10.1029/1999GL011268.

Cleaver, H., 1977: Malaria and the political economy of public health. *Int. J. Health Serv.*, **7**, 557–579, https://doi.org/10.2190/WXDB-Y7DN-FU49-DLFG.

Compo, G. P., and Coauthors, 2011: The Twentieth-Century Reanalysis Project. *Quart. J. Roy. Meteor. Soc.*, **137**, 1–28, https://doi.org/10.1002/qj.776.

Craig, M. H., R. W. Snow, and D. le Sueur, 1999: A climate-based distribution model of malaria transmission in sub-Saharan Africa. *Parasitol. Today*, **15**, 105–111, https://doi.org/10.1016/S0169-4758(99)01396-4.

Dayan, H., J. Vialard, T. Izumo, and M. Lengaigne, 2014: Does sea surface temperature outside the tropical Pacific contribute to enhanced ENSO predictability? *Climate Dyn.*, **43**, 1311–1325, https://doi.org/10.1007/s00382-013-1946-y.

Diouf, I., A. Deme, J.-A. Ndione, A. T. Gaye, B. Rodríguez-Fonseca, and M. Cisse, 2013: Climate and health: Observation and modeling of malaria in the Ferlo (Senegal). *C. R. Biol.*, **336**, 253–260, https://doi.org/10.1016/j.crvi.2013.04.001.

——, and Coauthors, 2017: Comparison of malaria simulations driven by meteorological observations and reanalysis products in Senegal. *Int. J. Environ. Res. Public Health*, **14**, 1119, https://doi.org/10.3390/ijerph14101119.

——, and Coauthors, 2020: Climate variability and malaria over West Africa. *Amer. J. Trop. Med. Hyg.*, **102**, 1037–1047, https://doi.org/10.4269/ajtmh.19-0062.

Ermert, V., A. H. Fink, A. E. Jones, and A. P. Morse, 2011: Development of a new version of the Liverpool Malaria Model. I. Refining the parameter settings and mathematical formulation of basic processes based on a literature review. *Malar. J.*, **10**, 35, https://doi.org/10.1186/1475-2875-10-35.

Folland, C. K., T. N. Palmer, and D. E. Parker, 1986: Sahelian rainfall and worldwide sea temperatures 1901–85. *Nature*, **320**, 602–607, https://doi.org/10.1038/320602a0.

Fontaine, B., S. Trzaska, and S. Janicot, 1998: Evolution of the relationship between near global and Atlantic SST modes and the rainy season in West Africa: Statistical analyses and sensitivity experiments. *Climate Dyn.*, **14**, 353–368, https://doi.org/10.1007/s003820050228.

Freeman, T., and M. Bradley, 1996: Temperature is predictive of severe malaria in Zimbabwe. *Trans. Roy. Soc. Trop. Med. Hyg.*, **90**, 232, https://doi.org/10.1016/S0035-9203(96)90224-2.

Gaetani, M., B. Fontaine, P. Roucou, and M. Baldi, 2010: Influence of the Mediterranean Sea on the West African monsoon: Intraseasonal variability in numerical simulations. *J. Geophys. Res.*, **115**, D24115, https://doi.org/10.1029/2010JD014436.

Gage, K. L., T. R. Burkot, R. J. Eisen, and E. B. Hayes, 2008: Climate and vector-borne diseases. *Amer. J. Prev. Med.*, **35**, 436–450, https://doi.org/10.1016/j.amepre.2008.08.030.

Gagnon, A. S., K. E. Smoyer-Tomic, and A. B. Bush, 2002: The El Niño Southern Oscillation and malaria epidemics in South America. *Int. J. Biometeor.*, **46**, 81–89, https://doi.org/10.1007/s00484-001-0119-6.

Giannini, A., R. Saravanan, and P. Chang, 2003: Oceanic forcing of Sahel rainfall on interannual to interdecadal time scales. *Science*, **302**, 1027–1030, https://doi.org/10.1126/science.1089357.

——, A. Ali, C. P. Kelley, B. L. Lamptey, B. Minoungou, and O. Ndiaye, 2020: Advances in the lead time of Sahel rainfall prediction with the North American multimodel ensemble. *Geophys. Res. Lett.*, **47**, e2020GL087341, https://doi.org/10.1029/2020GL087341.

Githeko, A. K., and W. Ndegwa, 2001: Predicting malaria epidemics in the Kenyan Highlands using climate data: A tool for decision makers. *Global Change Hum. Health*, **2**, 54–63, https://doi.org/10.1023/A:1011943131643.

Hagos, S. M., and K. H. Cook, 2008: Ocean warming and late-twentieth-century Sahel drought and recovery. *J. Climate*, **21**, 3797–3814, https://doi.org/10.1175/2008JCLI2055.1.

Hay, S. I., G. D. Shanks, D. I. Stern, R. W. Snow, S. E. Randolph, and D. J. Rogers, 2005: Climate variability and malaria epidemics in the highlands of East Africa. *Trends Parasitol.*, **21**, 52–53, https://doi.org/10.1016/j.pt.2004.11.007.

Hoshen, M. B., and A. P. Morse, 2004: A weather-driven model of malaria transmission. *Malar. J.*, **3**, 32, https://doi.org/10.1186/1475-2875-3-32.

Janicot, S., V. Moron, and B. Fontaine, 1996: Sahel droughts and ENSO dynamics. *Geophys. Res. Lett.*, **23**, 515–518, https://doi.org/10.1029/96GL00246.

——, A. Harzallah, B. Fontaine, and V. Moron, 1998: West African monsoon dynamics and eastern equatorial Atlantic and Pacific SST anomalies (1970–88). *J. Climate*, **11**, 1874–1882, https://doi.org/10.1175/1520-0442(1998)011<1874:WAMDAE>2.0.CO;2.

Jones, A., and A. Morse, 2010: Application and validation of a seasonal ensemble prediction system using a dynamic malaria

model. *J. Climate*, **23**, 4202–4215, https://doi.org/10.1175/2010JCLI3208.1.

Kalnay, E., and Coauthors, 1996: The NCEP/NCAR 40-Year Reanalysis Project. *Bull. Amer. Meteor. Soc.*, **77**, 437–471, https://doi.org/10.1175/1520-0477(1996)077<0437:TNYRP>2.0.CO;2.

Kiszewski, A. E., and A. Teklehaimanot, 2004: A review of the clinical and epidemiologic burdens of epidemic malaria. *Amer. J. Trop. Med. Hyg.*, **71** (2_Suppl.), 128–135, https://doi.org/10.4269/ajtmh.2004.71.128.

Korenromp, E. L., J. Miller, R. E. Cibulskis, M. Kabir Cham, D. Alnwick, and C. Dye, 2003: Monitoring mosquito net coverage for malaria control in Africa: Possession vs. use by children under 5 years. *Trop. Med. Int. Health*, **8**, 693–703, https://doi.org/10.1046/j.1365-3156.2003.01084.x.

Lindsay, S. W., and M. H. Birley, 1996: Climate change and malaria transmission. *Ann. Trop. Med. Parasitol.*, **90**, 573–588, https://doi.org/10.1080/00034983.1996.11813087.

Liu, K., H. Tsujimoto, S. J. Cha, P. Agre, and J. L. Rasgon, 2011: Aquaporin water channel AgAQP1 in the malaria vector mosquito *Anopheles gambiae* during blood feeding and humidity adaptation. *Proc. Natl. Acad. Sci. USA*, **108**, 6062–6066, https://doi.org/10.1073/pnas.1102629108.

Losada, T., B. Rodríguez-Fonseca, I. Polo, S. Janicot, S. Gervois, F. Chauvin, and P. Ruti, 2010a: Tropical response to the Atlantic equatorial mode: AGCM multimodel approach. *Climate Dyn.*, **35**, 45–52, https://doi.org/10.1007/s00382-009-0624-6.

——, ——, S. Janicot, S. Gervois, F. Chauvin, and P. Ruti, 2010b: A multi-model approach to the Atlantic equatorial mode: Impact on the West African monsoon. *Climate Dyn.*, **35**, 29–43, https://doi.org/10.1007/s00382-009-0625-5.

——, ——, E. Mohino, J. Bader, S. Janicot, and C. R. Mechoso, 2012: Tropical SST and Sahel rainfall: A non-stationary relationship. *Geophys. Res. Lett.*, **39**, L12705, https://doi.org/10.1029/2012GL052423.

Luterbacher, J., D. Dietrich, E. Xoplaki, M. Grosjean, and H. Wanner, 2004: European seasonal and annual temperature variability, trends, and extremes since 1500. *Science*, **303**, 1499–1503, https://doi.org/10.1126/science.1093877.

Mohino, E., S. Janicot, and J. Bader, 2011: Sahel rainfall and decadal to multidecadal sea surface temperature variability. *Climate Dyn.*, **37**, 419–440, https://doi.org/10.1007/s00382-010-0867-2.

Mordecai, E. A., and Coauthors, 2013: Optimal temperature for malaria transmission is dramatically lower than previously predicted. *Ecol. Lett.*, **16**, 22–30, https://doi.org/10.1111/ele.12015.

——, and Coauthors, 2019: Thermal biology of mosquito-borne disease. *Ecol. Lett.*, **22**, 1690–1708, https://doi.org/10.1111/ele.13335.

Morse, A. P., C. Caminade, A. E. Jones, D. MacLeod, and A. E. Heath, 2012: The QweCI project: Seamlessly linking climate science to society. *Geophysical Research Abstracts*, Vol. 14, Abstract EGU2012-1559, https://meetingorganizer.copernicus.org/EGU2012/EGU2012-1559.pdf.

Ndiaye, O., J. Y. Hesran, J. F. Etard, A. Diallo, F. Simondon, M. N. Ward, and V. Robert, 2001: Variations climatiques et mortalité attribuée au paludisme dans la zone de Niakhar, Sénégal, de 1984 à 1996. *Santé: Cah. Etud. Rech. Francophones*, **11**, 25–33.

Nicholson, S., 2005: On the question of the "recovery" of the rains in the West African Sahel. *J. Arid Environ.*, **63**, 615–641, https://doi.org/10.1016/j.jaridenv.2005.03.004.

——, and J. P. Grist, 2001: A conceptual model for understanding rainfall variability in the West African Sahel on interannual and interdecadal timescales. *Int. J. Climatol.*, **21**, 1733–1757, https://doi.org/10.1002/joc.648.

Ouédraogo, C. M. R., G. Nébié, L. Sawadogo, G. Rouamba, A. Ouédraogo, and J. Lankoandé, 2011: Étude des facteurs favorisant la survenue du paludisme à *Plasmodium falciparum* chez les femmes enceintes dans le district sanitaire de Bogodogo à Ouagadougou, Burkina Faso. *J. Gynecol. Obstet. Biol. Reprod.*, **40**, 529–534, https://doi.org/10.1016/j.jgyn.2011.03.005.

Patz, J. A., and S. H. Olson, 2006: Malaria risk and temperature: Influences from global climate change and local land-use practices. *Proc. Natl. Acad. Sci. USA*, **103**, 5635–5636, https://doi.org/10.1073/pnas.0601493103.

Pene, P., R. Baylet, and R. Michel, 1967: Le paludisme en zone sahélienne. *Med. Afr. Noire*, **14**, 187–231.

Philander, S. G. H., 1983: El Niño Southern Oscillation phenomena. *Nature*, **302**, 295–301, https://doi.org/10.1038/302295a0.

Poli, P. H., and Coauthors, 2016: ERA-20C: An atmospheric reanalysis of the twentieth century. *J. Climate*, **29**, 4083–4097, https://doi.org/10.1175/JCLI-D-15-0556.1.

Polo, I., B. Rodríguez-Fonseca, T. Losada, and J. García-Serrano, 2008: Tropical Atlantic variability modes (1979–2002). Part I: Time-evolving SST modes related to West African rainfall. *J. Climate*, **21**, 6457–6475, https://doi.org/10.1175/2008JCLI2607.1.

Poveda, G., W. Rojas, M. L. Quinones, I. D. Velez, R. I. Mantilla, D. Ruiz, J. S. Zuluaga, and G. L. Rua, 2001: Coupling between annual and ENSO timescales in the malaria climate association in Colombia. *Environ. Health Perspect.*, **109**, 489–493, https://doi.org/10.1289/ehp.01109489.

Prost, A., 1991: Les faits de santé aux cours et décours des sécheresses. *Sécheresse*, **2**, 40–47.

Rodrigues, P. T., and Coauthors, 2018: Human migration and the spread of malaria parasites to the New World. *Sci. Rep.*, **8**, 1993, https://doi.org/10.1038/s41598-018-19554-0.

Rodríguez-Fonseca, B., I. Polo, J. García-Serrano, T. Losada, E. Mohino, C. R. Mechoso, and F. Kucharski, 2009: Are Atlantic Niños enhancing Pacific ENSO events in recent decades?-*Geophys. Res. Lett.*, **36**, L20705, https://doi.org/10.1029/2009GL040048.

——, and Coauthors, 2011: Interannual and decadal SST forced responses of the West African monsoon. *Atmos. Sci. Lett.*, **12**, 67–74, https://doi.org/10.1002/asl.308.

——, and Coauthors, 2015: Variability and predictability of West African droughts: A review on the role of sea surface temperature anomalies. *J. Climate*, **28**, 4034–4060, https://doi.org/10.1175/JCLI-D-14-00130.1.

Rogers, D. J., and S. E. Randolph, 2000: The global spread of malaria in a future, warmer world. *Science*, **289**, 1763–1766, https://doi.org/10.1126/science.289.5485.1763.

Ropelewski, C. F., and M. S. Halpert, 1987: Global and regional scale precipitation patterns associated with the El Niño/Southern Oscillation. *Mon. Wea. Rev.*, **115**, 1606–1626, https://doi.org/10.1175/1520-0493(1987)115<1606:GARSPP>2.0.CO;2.

Rowell, D. P., 2001: Teleconnections between the tropical Pacific and the Sahel. *Quart. J. Roy. Meteor. Soc.*, **127**, 1683–1706, https://doi.org/10.1002/qj.49712757512.

——, 2003: The impact of Mediterranean SSTs on the Sahelian rainfall season. *J. Climate*, **16**, 849–862, https://doi.org/10.1175/1520-0442(2003)016<0849:TIOMSO>2.0.CO;2.

——, 2013: Simulating SST teleconnections to Africa: What is state of the art? *J. Climate*, **26**, 5397–5418, https://doi.org/10.1175/JCLI-D-12-00761.1.

Sachs, J., and P. Malaney, 2002: The economic and social burden of malaria. *Nature*, **415**, 680–685, https://doi.org/10.1038/415680a.

Smith, T. M., and R. W. Reynolds, 2003: Extended reconstruction of global sea surface temperatures based on COADS data (1854–1997). *J. Climate*, **16**, 1495–1510, https://doi.org/10.1175/1520-0442(2003)016<1495:EROGSS>2.0.CO;2.

——, and ——, 2004: Improved extended reconstruction of SST (1854–1997). *J. Climate*, **17**, 2466–2477, https://doi.org/10.1175/1520-0442(2004)017<2466:IEROS>2.0.CO;2.

——, ——, T. C. Peterson, and J. Lawrimore, 2008: Improvements to NOAA's historical merged land–ocean surface temperature analysis (1880–2006). *J. Climate*, **21**, 2283–2296, https://doi.org/10.1175/2007JCLI2100.1.

Suárez-Moreno, R., 2019: *Interdecadal Changes in Ocean Teleconnections with the Sahel: Implications in Rainfall Predictability*. Springer, 87 pp., https://doi.org/10.1007/978-3-319-99450-5.

——, and B. Rodríguez-Fonseca, 2015: S4CAST v2.0: Sea surface temperature based statistical seasonal forecast model. *Geosci. Model Dev.*, **8**, 3639–3658, https://doi.org/10.5194/gmd-8-3639-2015.

——, ——, J. A. Barroso, and A. H. Fink, 2018: Interdecadal changes in the leading ocean forcing of Sahelian rainfall interannual variability: Atmospheric dynamics and role of multidecadal SST background. *J. Climate*, **31**, 6687–6710, https://doi.org/10.1175/JCLI-D-17-0367.1.

Tompkins, A. M., and F. Di Giuseppe, 2015: Potential predictability of malaria in Africa using ECMWF monthly and seasonal climate forecasts. *J. Appl. Meteor. Climatol.*, **54**, 521–540, https://doi.org/10.1175/JAMC-D-14-0156.1.

——, F. J. Colón-González, and F. Di, 2019: Dynamical malaria forecasts are skillful at regional and local scales in Uganda up to 4 months ahead. *Geohealth*, **3**, 58–66, https://doi.org/10.1029/2018GH000157.

von Storch, H., and C. Frankignoul, 1998: Empirical modal decomposition in coastal oceanography. *The Global Coastal Ocean: Processes and Methods*, K. H. Brink and A. R. Robinson, Eds., *The Sea—Ideas and Observations on Progress in the Study of the Seas*, Vol. 10, John Wiley and Sons, 419–455.

——, and F. Zwiers, 2001: *Statistical Analysis in Climate Research*. Cambridge University Press, 484 pp.

Walker, S. P., and Coauthors, 2007: Child development: Risk factors for adverse outcomes in developing countries. *Lancet*, **369**, 145–157, https://doi.org/10.1016/S0140-6736(07)60076-2.

Wallace, J. M., and D. S Gutzler, 1981: Teleconnections in the geopotential height field during the Northern Hemisphere winter. *Mon. Wea. Rev.*, **109**, 784–812, https://doi.org/10.1175/1520-0493(1981)109<0784:TITGHF>2.0.CO;2.

Ward, M. N., 1992: Provisionally corrected surface wind data, worldwide ocean–atmosphere surface fields, and Sahelian rainfall variability. *J. Climate*, **5**, 454–475, https://doi.org/10.1175/1520-0442(1992)005<0454:PCSWDW>2.0.CO;2.

——, 1998: Diagnosis and short-lead time prediction of summer rainfall in tropical North Africa at interannual and multidecadal timescales. *J. Climate*, **11**, 3167–3191, https://doi.org/10.1175/1520-0442(1998)011<3167:DASLTP>2.0.CO;2.

Wilson, M. L., A. J. McMichael, A. Haines, R. Sloof, and S. Kovats, Eds., 1998: Climate change and human health. *Climatic Change*, **38**, 501–506, https://doi.org/10.1023/A:1005312531196.

World Health Organization, 2008: World malaria report 2008. WHO Rep., 190 pp., https://apps.who.int/iris/handle/10665/43939.

——, 2017: Population mobility and malaria. Regional Office for South-East Asia Rep., 120 pp., https://apps.who.int/iris/handle/10665/255816.

——, 2019: World malaria report 2019. WHO Rep., 232 pp., https://www.who.int/publications/i/item/9789241565721.

——, 2020: World malaria report 2020. WHO Rep., 299 pp., https://www.who.int/publications/i/item/9789240015791.